The Astrophysical Journal Letters, 732:L20 (5pp), 2011 May 10 doi:10.1088/2041-8205/732/2/L20

FIRST EVIDENCE OF COEXISTING EIT WAVE AND CORONAL MORETON WAVE FROM *SDO*/AIA OBSERVATIONS

P. F. Chen[1,2] and Y. Wu[1,2]
[1] Department of Astronomy, Nanjing University, Nanjing 210093, China; chenpf@nju.edu.cn
[2] Key Lab of Modern Astronomy & Astrophysics (Ministry of Education), Nanjing University, China
Received 2011 March 1; accepted 2011 March 31; published 2011 April 13

ABSTRACT

"EIT waves" are a globally propagating wavelike phenomenon. They were often interpreted as fast-mode magnetoacoustic waves in the corona, despite various discrepancies between the fast-mode wave model and observations. To reconcile these discrepancies, we suggested that "EIT waves" are the apparent propagation of the plasma compression due to successive stretching of the magnetic field lines pushed by the erupting flux rope. According to this model, an EIT wave should be preceded by a fast-mode wave, which, however, had rarely been observed. With the unprecedented high cadence and sensitivity of the *Solar Dynamics Observatory* observations, we discern a fast-moving wave front with a speed of 560 km s^{-1} ahead of an EIT wave, which had a velocity of ~190 km s^{-1}, in the "EIT wave" event on 2010 July 27. The results, suggesting that "EIT waves" are not fast-mode waves, confirm the prediction of our field-line stretching model for an EIT wave. In particular, it is found that the coronal Moreton wave was ~3 times faster than the EIT wave, as predicted.

Key words: Sun: corona – Sun: coronal mass ejections (CMEs) – waves

Online-only material: animation, color figures

1. INTRODUCTION

Any perturbation, from small-scale convective motions to large-scale eruptions, can generate waves propagating in the solar atmosphere. According to the magnetohydrodynamic (MHD) theory, they can be identified in terms of fast-mode, Alfvénic, or slow-mode waves. For instance, Hα Moreton waves were successfully explained as coronal fast-mode waves sweeping the chromosphere (Uchida 1968). After the launch of the *Solar and Heliospheric Observatory* (*SOHO*) spacecraft, the EUV Imaging Telescope (EIT) discovered a large-scale wavelike phenomenon, which was later called an "EIT wave" (Moses et al. 1997; Thompson et al. 1998).

"EIT waves" are bright fronts visible in the EUV difference images, propagating with a typical velocity of 170–350 km s^{-1} (Klassen et al. 2000). Although the velocity might be underestimated due to the low cadence of the EIT telescope (Long et al. 2008), it can actually be as small as ~10 km s^{-1} (Zhukov et al. 2009). In the base difference images, EIT waves are followed by extending dimmings (Thompson et al. 2000). Upon discovery, EIT waves were soon explained as the fast-mode magnetoacoustic waves, i.e., the coronal counterparts of Hα Moreton waves (or coronal Moreton waves; Thompson et al. 1998). Subsequent models (Wang 2000; Wu et al. 2001) and observations (Vršnak et al. 2002; Warmuth et al. 2004; Ballai et al. 2005; Grechnev et al. 2008; Pomoell et al. 2008; Veronig et al. 2008; Gopalswamy et al. 2009; Patsourakos & Vourlidas 2009) further claimed that the fast-mode wave model can account for the EIT waves. Such a fast-mode wave model was first questioned by Delannée & Aulanier (1999), since they found that an EIT wave stopped at the magnetic separatrix, which is hard to explain in the wave model. The second drawback of the fast-mode wave model is that the EIT wave speed is typically ~3 times smaller than that of Moreton waves (Klassen et al. 2000). In addition, it was found that the EIT wave front is cospatial with the coronal mass ejection (CME) frontal loop (Attrill et al. 2009; Chen 2009a; Dai et al. 2010), which is not expected from the fast-mode wave model. In order to reconcile these discrepancies, several alternative models have been proposed, e.g., the field-line stretching model (Chen et al. 2002, 2005), the successive reconnection model (Attrill et al. 2007), the slow-mode wave model (Wills-Davey 2006; Wang et al. 2009), the current sheet model (Delannée et al. 2008), amongst others (see Wills-Davey & Attrill 2009; Gallagher & Long 2010; Warmuth 2010, for reviews).

According to the field-line stretching model of Chen et al. (2002, 2005), a fast-mode wave should be ahead of the EIT wave in a CME event, providing that the observational cadence and sensitivity are high enough. In particular, the model predicts that the fast-mode wave is ~3 times faster than the EIT wave if the magnetic configuration is semicircular. The coexistence of a faster wave (500 km s^{-1} in speed) ahead of an EIT wave (200 km s^{-1} in speed) was discovered by Harra & Sterling (2003) with the *Transition Region and Coronal Explorer* (*TRACE*) observations. In this Letter, we report the evidence of a coexisting faster wave ahead of the slower EIT wave on 2010 July 27, which was observed by the newly launched *Solar Dynamics Observatory* (*SDO*) mission.

2. DATA ANALYSIS

On 2010 July 27, a microflare with the Solar Object Locator of SOL2010-07-27T08:46:00L223C108 occurred to the west side of NOAA Active Region 11089 (S24W21). The microflare was located at S18W48. The *GOES* 1–8 Å soft X-ray light curve shows a small enhancement less than A2 level from 08:46 UT to 08:56 UT. Accompanying the occurrence of the tiny flare, EUV waves and dimmings can be identified in the base difference images, extending from the flare site to the north for a short distance. No coronagraph observations from the *SOHO* satellite are available. The microflare was located at S22E31 in the field of view of the *Solar TErrestrial RElations Observatory* (*STEREO*; Kaiser et al. 2008) *A* satellite, and its coronagraphs did not detect any CME during this event. Two factors do not

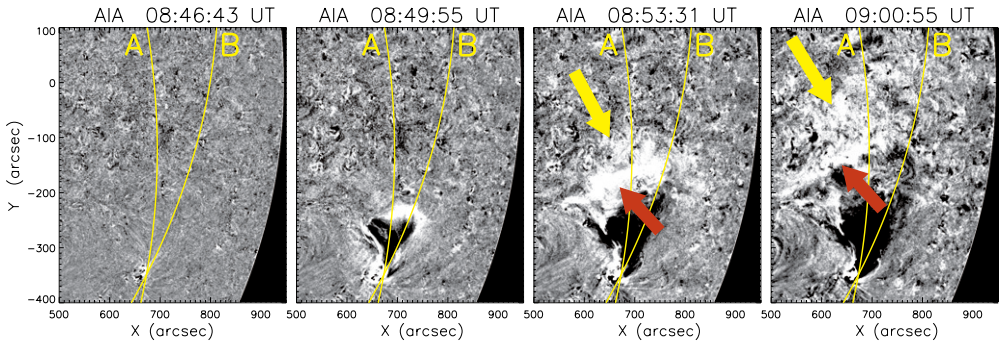

Figure 1. Sequential difference images of the 2010 July 27 event observed by *SDO*/AIA at 193 Å where the intensity map at 08:44:55 UT is subtracted. The white/dark pixels indicate intensity increase/decrease. The red arrows point to the fronts of the slower EIT wave, whereas the yellow arrows to the fast-mode wave. Two slices, A and B, are great circles linking the flare site at (670″, −350″). Note that there exists a small coronal loop at (720″, −200″). The corresponding animation is included as online material.

(An animation and a color version of this figure are available in the online journal.)

favor the detection of a possible CME: (1) the source region is too close to the solar disk center for the *STEREO* satellite; (2) the CME, if it existed, should have a small angular extension as implied by the EUV dimmings, and therefore is prone to be missed by coronagraphs (Zhang et al. 2010).

This event was well documented by the Atmospheric Imaging Assembly (AIA) on the *SDO* spacecraft (Title et al. 2006). The AIA instrument has 10 EUV and UV channels with a spatial resolution of 1.″2. Since EIT waves are most evident at the 193 Å channel, we mainly use this channel in this Letter. The cadence of the observation is 12 s, which allows the detection of the detailed features of EIT waves that had not been seen before (Liu et al. 2010).

In order to clearly show the propagation of faint EIT waves, running or base difference technique was often used. Throughout this Letter, we rely on the percentage difference images, which are obtained by the base difference images divided by the pre-event image (Wills-Davey & Thompson 1999). The rotation of the Sun is corrected. For simplicity, the percentage difference images are mentioned as difference images hereafter.

3. RESULTS

The evolution of the EIT wave event on 2010 July 27 is displayed in Figure 1, which shows the 193 Å difference images at four moments. The pre-event intensity map at 08:44:55 UT is chosen as the base image that is subtracted. In this figure, the bright (dark) pixels indicate the intensity increase (decrease). At 08:46:43 UT, a small-sized brightening occurred near (670″, −350″). Note that a small coronal loop with relatively stronger magnetic field was located north at around (720″, −200″), which is clearly seen in the second panel. Shortly later, bright fronts appeared and began to propagate to the north. It is revealed from the animation associated with Figure 1 that the western and eastern flanks formed first. At 08:49:55 UT, the northern flank became dominant in brightness. Until this stage, only one bright strip was evident along the northern flank. At 08:53:31 UT, the northern flank of the brightenings swept over the small coronal loop, and was then separated, presumably due to the small coronal loop. On the east side, a weak front became detached ahead of the main strip, as indicated by the yellow and red arrows, respectively, in the third panel of Figure 1. The weak front propagated much faster than the main strip, and the two fronts were widely separated at 09:00:55 UT, as illustrated by the right panel of Figure 1. On the west side, only a bright strip is discernable by eye, which propagated quickly.

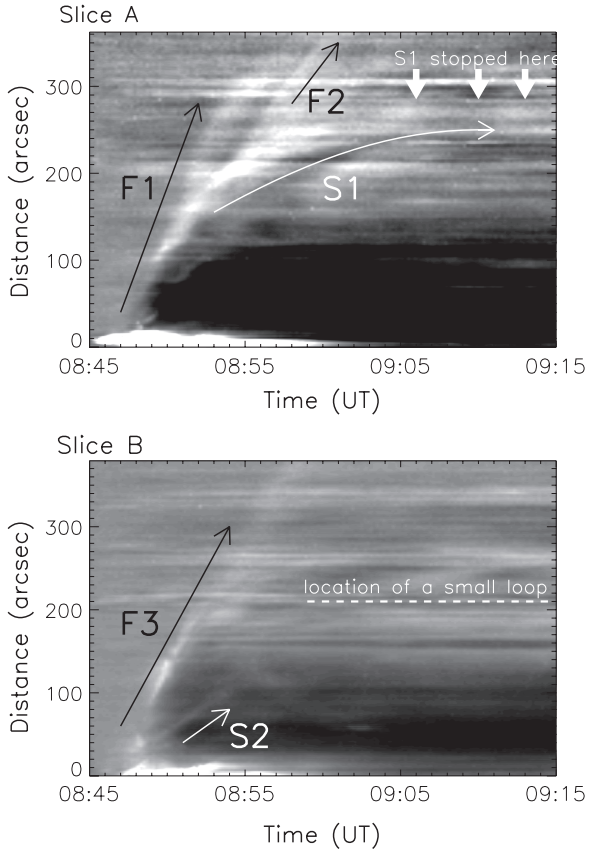

Figure 2. Time evolutions of the 193 Å difference intensity distributions along slice A (top) and along slice B (bottom). The trajectories of slices A and B are marked in Figure 1, and the distance is measured along the slice from the flare site. Wave patterns are indicated by the arrows, with the corresponding speeds of F1 $\sim$ 560 km s^{-1}, F2 $\sim$ 310 km s^{-1}, S1 $\lesssim$ 190 km s^{-1}, F3 $\sim$ 470 km s^{-1}, and S2 $\sim$ 170 km s^{-1}.

In order to investigate the dynamics of the wave fronts more quantitatively, we analyze the time evolution of the brightness distributions along two slices, A and B, which are separated by the small coronal loop at (720″, −200″) as indicated in Figure 1. The two slices are both great circles along the solar surface linking the flare site. The results are displayed in Figure 2 as a space–time plot, where any oblique pattern signifies a propagating front.

The top panel of Figure 2 displays the evolution of the wave front propagation along slice A. We can identify several fronts:

F1, F2, and S1. Front F1 appeared first, which propagated with a high velocity of 560 km s^{-1} until 08:52:44 UT. The extrapolated potential magnetic field at 1.2 $R_\odot$ is 2.5 G, which leads to the Alfvén speed of 540 km s^{-1}. The sound speed at the formation temperature of 193 Å, i.e., 1.5 MK, is 186 km s^{-1}. The resulting fast-mode wave speed across the field line is $\sqrt{540^2 + 186^2} = 571$ km s^{-1}, which is very close to speed of front F1. Therefore, we interpret front F1 as a fast-mode wave. A separate bright front S1 was propagating with an initial speed of 190 km s^{-1} since 08:52:00 UT. Its speed was decreasing. After 09:02:28 UT, front S1 stopped at a distance of ∼253″ from the flare site. Since its speed even decreased below the sound speed, it cannot be a fast-mode wave. It is a typical EIT wave. Front S1 might already exist during the period from 08:49:04 UT to 08:52:00 UT, but it is almost indistinguishable from the fast front F1 in Figure 2. It is interesting to see that an additional wave pattern, front F2, emanated from front S1 at the distance of ∼220″ from the flare site at 08:54:54 UT. This weak front propagated with a speed of 310 km s^{-1}. We interpret it as a fast-mode wave because (1) it is much faster than the sound speed; (2) after a distance of ∼270″ the fast front F1 began to decelerate and propagated with almost the same speed as front F2; and (3) it was not affected by the magnetic separatrix.

The bottom panel of Figure 2 illustrates the wave front propagation along slice B. The wave pattern here is very simple. Besides a fast-moving bright front, F3, which had a velocity of 470 km s^{-1}, there is a weak front, S2, propagating outward with a velocity of 170 km s^{-1}. With the same reasons for fronts F1 and S1, we identify the faster front F3 as a fast-mode wave and the slower front S2 as an EIT wave.

4. DISCUSSIONS

4.1. Identification of an EIT Wave and Coronal Moreton Wave

Since the discovery, EIT waves were widely explained as fast-mode waves, or coronal Moreton waves. However, many of their characteristics cannot be explained in the framework of fast-mode waves, which stimulated Delannée (2000) to doubt the wave nature of the EIT waves. Based on MHD simulations, Chen et al. (2002, 2005) proposed a magnetic field-line stretching model, i.e., EIT waves are not fast-mode waves, but are the apparent propagation of the brightenings from the compressed plasma generated by successive stretching of the magnetic field lines overlying the erupting flux rope. The model predicts that there should be a sharp fast-mode wave, or coronal Moreton wave, which is piston-driven by the erupting flux rope and propagates ahead of the EIT waves. The speed of the faster wave is just the local fast-mode magnetoacoustic wave speed; however, the EIT wave speed is determined by both local parameters and the magnetic configuration. According to this model, if the coronal magnetic field lines are semicircles, the EIT wave should be ∼3 times slower than the fast-mode wave. If the coronal field has a strongly stretched configuration, the resulting EIT wave has a very low speed (Chen 2009b; Yang & Chen 2010) and is close to zero near a magnetic separatrix. Such a field-line stretching model, which was originally based on two-dimensional simulations, was recently backed by three-dimensional simulations (Downs et al. 2011).

Chen et al. (2002, 2005) pointed out that the coronal Moreton waves are so fast that at most one front can be detected with the low-cadence (∼15 minutes) observations of the *SOHO*/EIT telescope; e.g., the sharp front in Figure 1 of Thompson et al. (2000) is a coronal Moreton wave front. Their propagation can be caught only with a higher cadence. However, even with a cadence of 2.5 minutes, the Extreme Ultraviolet Imager (EUVI) on board *STEREO* still has not detected a coronal Moreton wave ahead of any EIT wave. Up to now, the existence of a coronal Moreton wave ahead of the EIT wave was implied by the filament winking (Eto et al. 2002), and the only direct evidence was revealed by Harra & Sterling (2003) with the *TRACE* observations, though Wills-Davey (2006) had a different opinion. According to Section 3, it is seen that the high-resolution observations of the *SDO*/AIA telescope revealed that there is another faster wave propagating ahead of the slower wave, either along slice A or slice B as marked in Figure 1. We interpret the slower waves, i.e., fronts S1 and S2 in Figure 2, as EIT waves, and the faster waves, i.e., fronts F1–F3 in Figure 2, as the fast-mode wave or coronal Moreton wave.

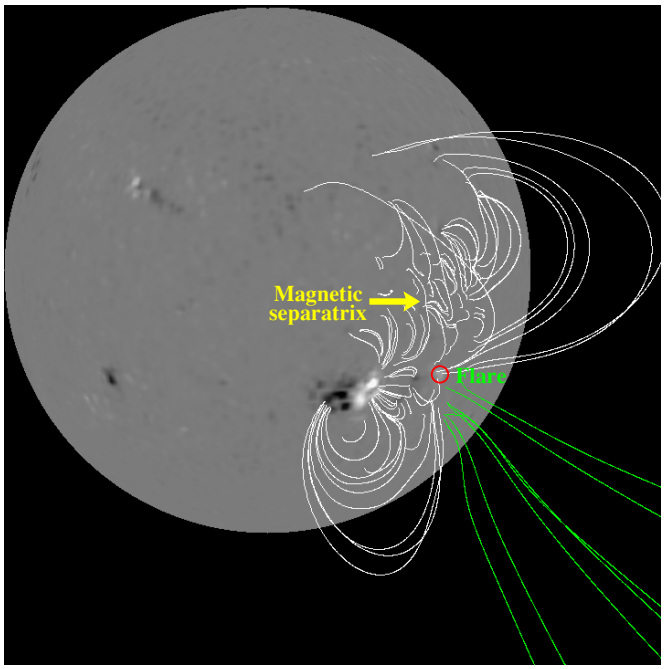

Figure 3. Coronal magnetic field distribution near the eruption site, which is extrapolated from the *SOHO*/MDI magnetogram with the Potential Field Source-Surface model. The yellow arrow points to a magnetic separatrix.
(A color version of this figure is available in the online journal.)

Along slice A, the top panel of Figure 2 clearly shows that the slower front S1 propagated outward with bright and diffuse fronts (∼30″ in width) and with an initial speed of 190 km s^{-1}, which are the typical characteristics of EIT waves (Klassen et al. 2000). During the propagation, the front S1 decelerated, and became almost stationary after 09:02:40 UT, when the front was at a distance of 250″ from the flare site. Previously, Delannée & Aulanier (1999) found that EIT waves stop at the footpoints of a magnetic separatrix. This feature was successfully explained by Chen et al. (2005, 2006) in terms of the field-line stretching model, i.e., the magnetic field across the magnetic separatrix belongs to another flux system, and hence are not involved in the stretching process. Therefore, EIT waves cannot go across the magnetic separatrix. To confirm such a conclusion, we plot in Figure 3 the coronal magnetic field near the eruption site, which is extrapolated based on the *SOHO*/Michelson Doppler Imager (MDI) magnetogram (Scherrer et al. 1995) with the Potential Field Source-Surface model (Schrijver & De Rosa 2003). The arrow in the figure points to the location where the EIT wave

front stopped. We can see that it is indeed cospatial with the magnetic separatrix.

The front F1 in the top panel of Figure 2, which we suggest is fast-mode wave in nature, should not be affected by the existence of the magnetic separatrix at the distance of 250″ from the flare site. It propagated across it, though its speed decreased (due to weaker magnetic field) as inferred from its declined slope in the top panel of Figure 2. However, one feature that is not expected is the second fast wave front F2 in the top panel of Figure 2. Apparently it emanated from the bright EIT wave front at 08:55:00 UT when the EIT wave front was at a distance of ∼220″ from the flare site. Checking the EUV images in Figure 1, we find that there is a small-sized coronal loop situated at such a distance with a relatively stronger magnetic field. Therefore, we hypothesize that the front F2 is due to the fast-mode wave near the west side of the small coronal loop being diffracted to propagate to the east. This is reinforced by the animation associated with Figure 1.

Along slice B, the bottom panel of Figure 2 presents a bright front (F3) with a propagation speed of 470 km s^{-1} and another faint front behind (S2) with a speed of 170 km s^{-1}. Apparently the faster wave seems to be an ordinary EIT wave in the sense that dimmings were behind. However, we interpret it as a fast-mode wave, because it was moving together with the fast-mode wave on slice A with a speed comparable to the local fast-mode wave speed. Besides, there is a very faint reflected wave in the bottom panel of Figure 2 when the faster wave F2 approached the small coronal loop at 08:52:30 UT, which is a typical characteristic of fast-mode waves. Moreover, this faster wave has sharper fronts (∼20″ in width). Determining the nature of the slower front S2 is not straightforward since it was so weak that it is not discernable from the difference images in Figure 1. Since this front had a typical speed for EIT waves, we tentatively explain it as an EIT wave. It is seen that the EIT wave front along slice B was much weaker than that along slice A. The reason is that the magnetic field lines overlying the eruption site were mainly oriented along the direction of slice A (see Figure 3). According to the field-line stretching model of Chen et al. (2002, 2005), as these field lines are pushed to stretch up, compression would be formed at the legs of these field lines. Therefore, bright EIT wave fronts are visible along slice A. The fast-mode wave, however, is always refracted toward the region with weak magnetic field (Uchida 1968) and has nothing to do with the magnetic connectivity. This is why the coronal Moreton wave is extremely bright along slice B (where the magnetic field is weak) and faint along slice A. It is noticed that dimmings were visible between fronts F3 and S2, though they are not as strong as the dimmings behind front S2. They might be due to plasma rarefaction behind the fast-mode wave.

It is interesting to note that, either along slice A or slice B, the coronal Moreton wave was moving with a speed ∼3 times higher than that of the following EIT wave, consistent with the prediction of the field-line stretching model of Chen et al. (2002, 2005) when semicircular magnetic configuration is assumed.

4.2. Why Were Fast-mode Waves Missed Before?

Chen et al. (2002, 2005) predicted that the fast-mode wave ahead of the EIT wave was missed by *SOHO*/EIT due to its low cadence of ∼15 minutes, and would be observed with a higher cadence. However, after the launch of the *STEREO* mission, the EUVI instrument with a high cadence of 2.5 minutes still did not catch the fast-mode wave (Wills-Davey & Attrill 2009).

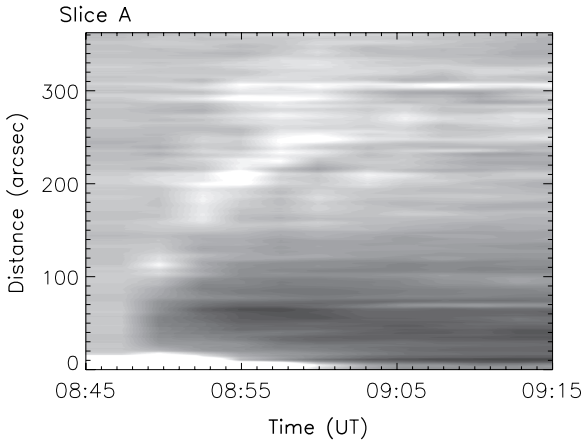

Figure 4. Time evolution of the 193 Å difference intensity distribution along slice A, which is a reproduction of the top panel of Figure 2 but with a degraded cadence of 2.5 minutes.

To check the eligibility of *STEREO*/EUVI in detecting the possible fast-mode wave ahead of the EIT wave, we degrade the temporal resolution of the top panel of Figure 2 from 12 s to 2.5 minutes and replot it in Figure 4. It is seen that the wave pattern becomes messy, and we cannot distinguish a faster wave from the EIT wave. This means that, for an EIT wave event like that on 2010 July 27, the 2.5 minute cadence imaging observations even with a spatial resolution of 1.″2 cannot detect the fast-mode wave ahead of the EIT wave. We further find that only if the observational cadence is shorter than 70 s can the fast-mode wave be distinguished from the EIT wave for the 2010 July 27 event.

With *STEREO*/EUVI observations, Cohen et al. (2009) did show a weak fast-mode wave component as well as the ordinary EIT wave. They found that the fast-mode wave was coupled with the EIT wave when the CME was expanding laterally, and the two waves ultimately decoupled when the EIT wave front became stationary. Such a result may result from the low cadence of the *STEREO*/EUVI data, as people can get the same impression from Figure 4. With a high cadence of 12 s, Figure 2 clearly reveals that the fast-mode wave was already distinct from the EIT wave front before the EIT wave stopped.

To summarize, we analyzed the EIT wave event on 2010 July 27 with the *SDO*/AIA data. It is seen that even for a tiny flare, the high-resolution observations of the *SDO*/AIA telescope still revealed many wave patterns. In this Letter, we found a fast-mode magnetoacoustic wave propagating ahead of the EIT wave. As predicted by the field-line stretching model of Chen et al. (2002, 2005), the fast-mode wave had a speed ∼3 times higher than that of the EIT wave. The fast-mode wave kept propagating after the EIT wave stopped at the magnetic separatrix. Our results are strongly suggestive that EIT waves are not fast-mode waves, and can be explained by our field-line stretching model.

The authors thank A. Title and N. Nitta for discussions and the AIA team for providing the calibrated data. *SOHO* is a project of international cooperation between ESA and NASA. This research is supported by the Chinese foundations 2011CB811402 and NSFC (10403003, 10933003, and 10673004).

REFERENCES

Attrill, G. D. R., Engell, A. J., Wills-Davey, M. J., Grigis, P., & Testa, P. 2009, ApJ, 704, 1296

Attrill, G. D. R., Harra, L. K., van Driel-Gesztelyi, L., & Démoulin, P. 2007, ApJ, 656, L101
Ballai, I., Erdélyi, R., & Pintér, B. 2005, ApJ, 633, L145
Chen, P. F. 2009a, ApJ, 698, L112
Chen, P. 2009b, Sci. China G, 52, 1785
Chen, P. F., Fang, C., & Shibata, K. 2005, ApJ, 622, 1202
Chen, P. F., Fang, C., & Shibata, K. 2006, Adv. Space Res., 38, 456
Chen, P. F., Wu, S. T., Shibata, K., & Fang, C. 2002, ApJ, 572, L99
Cohen, O., Attrill, G. D. R., Manchester, W. B., & Wills-Davey, M. J. 2009, ApJ, 705, 587
Dai, Y., Auchère, F., Vial, J.-C., Tang, Y. H., & Zong, W. G. 2010, ApJ, 708, 913
Delannée, C. 2000, ApJ, 545, 512
Delannée, C., & Aulanier, G. 1999, Sol. Phys., 190, 107
Delannée, C., Török, T., Aulanier, G., & Hochedez, J.-F. 2008, Sol. Phys., 247, 123
Downs, C., Roussev, I. I., van der Holst, B., Lugaz, N., Sokolov, I. V., & Gombosi, T. I. 2011, ApJ, 728, 2
Eto, S., et al. 2002, PASJ, 54, 481
Gallagher, P. T., & Long, D. M. 2010, Space Sci. Rev., 135
Gopalswamy, N., et al. 2009, ApJ, 691, L123
Grechnev, V. V., Uralov, A. M., Slemzin, V. A., Chertok, I. M., Kuzmenko, I. V., & Shibasaki, K. 2008, Sol. Phys., 253, 263
Harra, L. K., & Sterling, A. C. 2003, ApJ, 587, 429
Kaiser, M. L., Kucera, T. A., Davila, J. M., St. Cyr, O. C., Guhathakurta, M., & Christian, E. 2008, Space Sci. Rev., 136, 5
Klassen, A., Aurass, H., Mann, G., & Thompson, B. J. 2000, A&A, 141, 357
Liu, W., Nitta, N. V., Schrijver, C. J., Title, A. M., & Tarbell, T. D. 2010, ApJ, 723, L53
Long, D. M., Gallagher, P. T., McAteer, R. T. J., & Bloomfield, D. S. 2008, ApJ, 680, L81
Moses, D., et al. 1997, Sol. Phys., 175, 571
Patsourakos, S., & Vourlidas, A. 2009, ApJ, 700, 182
Pomoell, J., Vainio, R., & Kissmann, R. 2008, Sol. Phys., 253, 249
Scherrer, P. H., et al. 1995, Sol. Phys., 162, 129
Schrijver, C. J., & De Rosa, M. L. 2003, Sol. Phys., 212, 165
Thompson, B. J., Plunkett, S. P., Gurman, J. B., Newmark, J. S., St. Cyr, O. C., & Michels, D. J. 1998, Geophys. Res. Lett., 25, 2465
Thompson, B. J., Reynolds, B., Aurass, H., Gopalswamy, N., Gurman, J. B., Hudson, H. S., Martin, S. F., & St. Cyr, O. C. 2000, Sol. Phys., 193, 161
Title, A. M., Hoeksema, J. T., Schrijver, C. J., & Schrijver, C. J. The Aia Team 2006, 36th COSPAR Scientific Assembly, 2600
Uchida, Y. 1968, Sol. Phys., 4, 30
Veronig, A. M., Temmer, M., & Vršnak, B. 2008, ApJ, 681, L113
Vršnak, B., Warmuth, A., Brajša, R., & Hanslmeier, A. 2002, A&A, 394, 299
Wang, H., Shen, C., & Lin, J. 2009, ApJ, 700, 1716
Wang, Y. M. 2000, ApJ, 543, L89
Warmuth, A. 2010, Adv. Space Res., 45, 527
Warmuth, A., Vršnak, B., Magdalenić, J., Hanslmeier, A., & Otruba, W. 2004, A&A, 418, 1117
Wills-Davey, M. J. 2006, ApJ, 645, 757
Wills-Davey, M. J., & Attrill, G. D. R. 2009, Space Sci. Rev., 149, 325
Wills-Davey, M. J., & Thompson, B. J. 1999, Sol. Phys., 190, 467
Wu, S. T., Zheng, H., Wang, S., Thompson, B. J., Plunkett, S. P., Zhao, X. P., & Dryer, M. 2001, J. Geophys. Res., 106, 25089
Yang, H. Q., & Chen, P. F. 2010, Sol. Phys., 266, 59
Zhang, Q.-M., Guo, Y., Chen, P.-F., Ding, M.-D., & Fang, C. 2010, Res. Astron. Astrophys., 10, 461
Zhukov, A. N., Rodriguez, L., & de Patoul, J. 2009, Sol. Phys., 259, 73